Tryptophan Fluorescence Monitors Multiple Conformational Changes Required for Glutamine Phosphoribosylpyrophosphate Amidotransferase Interdomain Signaling and Catalysis[†,‡]

Sihong Chen,[§] John W. Burgner,[||] Joseph M. Krahn,[||,⊥] Janet L. Smith,[||] and Howard Zalkin*[,§]

Departments of Biochemistry and Biological Sciences, Purdue University, West Lafayette, Indiana 47907

Received May 10, 1999; Revised Manuscript Received June 25, 1999

ABSTRACT: Single tryptophan residues were incorporated into each of three peptide segments that play key roles in the structural transition of ligand-free, inactive glutamine phosphoribosylpyrophosphate (PRPP) amidotransferase to the active enzyme−substrate complex. Intrinsic tryptophan fluorescence and fluorescence quenching were used to monitor changes in a phosphoribosyltransferase (PRTase) "flexible loop", a "glutamine loop", and a C-terminal helix. Steady state fluorescence changes resulting from substrate binding were used to calculate binding constants and to detect the structural rearrangements that coordinate reactions at active sites for glutamine hydrolysis and PRTase catalysis. Pre-steady state kinetics of enzyme·PRPP and enzyme·PRPP·glutamine complex formation were determined from stopped-flow fluorescence measurements. The kinetics of the formation of the enzyme·PRPP complex were consistent with a model with two or more steps in which rapid equilibrium binding of PRPP is followed by a slow enzyme isomerization. This isomerization is ascribed to the closing of the PRTase flexible loop and is likely the rate-limiting step in the reaction of PRPP with NH_3. The pre-steady state kinetics for binding glutamine to the binary enzyme·PRPP complex could also be fit to a model involving rapid equilibrium binding of glutamine followed by an enzyme isomerization step. The changes monitored by fluorescence account for the interconversions between "end state" structures determined previously by X-ray crystallography and define an intermediate enzyme·PRPP conformer.

Glutamine PRPP[1] amidotransferase catalyzes the initial reaction in the pathway for de novo synthesis of purine nucleotides. The enzyme consists of an N-terminal glutaminase domain that defines an Ntn class of amidotransferases (*1*, *2*) and a C-terminal PRTase domain characteristic of type I PRTases (*3*). The overall reaction, shown in eq 1, thus involves catalysis at active sites in two separate domains.

$$\text{glutamine} + \text{PRPP} + H_2O \rightarrow \text{PRA} + \text{glutamate} + PP_i \quad (1)$$

$$\text{glutamine} + H_2O \rightarrow \text{glutamate} + NH_3 \quad (2)$$

$$NH_3 + \text{PRPP} \rightarrow \text{PRA} + PP_i \quad (3)$$

The reactions at the two active sites are given by eqs 2 and 3. Hydrolysis of glutamine at the glutaminase site (eq 2) is followed by transfer of NH_3 to the PRPP site where synthesis of PRA takes place (eq 3). Like most glutamine amidotransferases (*4*), the enzyme can also utilize external NH_3 as a nitrogen source for PRA synthesis, both in vitro and in vivo. This reaction is also represented by eq 3. There are important implications for an NH_3-mediated nitrogen transfer mechanism as shown by eqs 2 and 3. First, it is necessary to sequester enzyme-bound NH_3 from H_2O since NH_4^+ is not a substrate. Then the NH_3 must be transferred between the two physically separated active sites. Finally, the activities at the two sites must be coordinated to maintain a 1:1:1 stoichiometry between glutamine and PRPP consumed as reactants and PRA produced.

X-ray structures of glutamine PRPP amidotransferase from *Bacillus subtilis* (*5*) and *Escherichia coli* (*6*) have defined the glutaminase and PRTase domains. While informative, these substrate-free enzyme conformers have structural features that are incompatible with catalysis. In brief, the glutamine site is closed and inaccessible to glutamine, the PRPP site is open to solvent, thereby exposing PRPP to hydrolysis, and there is a 16 Å solvent accessible space separating the two sites. These barriers to catalysis are not present in the X-ray structure of an *E. coli* enzyme with substrate analogues bound (*7*). In the ternary complex, cPRPP is bound to the PRPP site and DON is covalently attached to Cys1 to mimic the glutamyl thioester catalytic intermediate. Ordering of a PRTase "flexible loop" closes off the PRPP site and forms an NH_3 channel connecting the glutamine and PRPP sites. Thus, the overall reaction shown by eq 1 indeed proceeds in two steps at physically separated catalytic sites

[†] Supported by NIH Grant DK42303 to J.L.S. and NIH Grant GM24268 to H.Z.

[‡] This is journal paper 16023 from the Purdue University Agricultural Research Station.

* To whom correspondence should be addressed.

[§] Department of Biochemistry.

[||] Department of Biological Sciences.

[⊥] Present address: National Institute of Environmental Health Sciences, NIH, Research Triangle Park, NC 27709.

[1] Abbreviations: PRPP, 5-phosphoribosyl-(∝) 1-pyrophosphate; cPRPP, carbocyclic 5-phosphoribosyl-(∝) 1-pyrophosphate; PRA, 5-phosphoribosyl-(*β*) 1-amine; PRTase, phosphoribosyl transferase; DON, 6-diazo-5-oxonorleucine; GAR, glycinamide ribonucleotide.

10.1021/bi991060o CCC: $18.00
Published on Web 08/17/1999

having tightly coupled activities. Catalytic coupling ensures that glutaminase activity is suppressed until PRPP is bound and is available to accept NH_3 (*8*). The glutamine PRPP amidotransferase X-ray structures define end point conformational states for a ligand-free enzyme and an enzyme−substrate analogue ternary complex, but they provide no information about dynamics in the structural transition or about possible intermediate conformational states.

To monitor the conformational transition between inactive and active states and to search for additional intermediate states, we have engineered enzymes having a single tryptophan residue in each of three peptides shown by the X-ray structures to undergo important changes in conformation. Analyses of intrinsic steady state and pre-steady state tryptophan fluorescence changes further define conformational transitions and discernible intermediate steps required for catalysis. The new data support the recently proposed structure-based mechanism (*9*, *10*) for catalysis and provide evidence for the enzyme•PRPP conformer that catalyzes the reaction of external NH_3 with PRPP or can bind glutamine to form the ternary complex.

EXPERIMENTAL PROCEDURES

Plasmids. Phagemid pETpurF was constructed for *purF* mutagenesis and for overexpression. The *E. coli purF* gene encoding glutamine PRPP amidotransferase was excised from pT7F1 (*11*) using *Xba*I and was ligated into the *Xba*I site of phagemid pET24a (Novagen) to yield pETpurF. Mutations were constructed by the method of Kunkel et al. (*12*) using pETpurF phagemid DNA. Plasmid pETEG was constructed for production of *E. coli* GAR synthetase. *E. coli purD* encoding GAR synthetase (*13*) was cloned by PCR from chromosomal DNA and ligated into plasmid pET24a at the *Nde*I and *Bam*HI sites.

Enzyme Production and Purification. Glutamine PRPP amidotransferase was accumulated in *E. coli* strain B834 (*14*) transformed with a plasmid encoding either the wild type or a mutant enzyme. Cells were grown at 37 °C in 2 L flasks containing 1 L of Luria broth containing 50 μg/mL kanamycin. Flasks were inoculated with 10 mL of culture, and the cultures were grown for 16−18 h without induction. Using these growth conditions, the enzyme accounted for approximately 50% of the soluble protein. Cells from 2 L of medium were harvested by centrifugation, washed with PBS buffer containing 0.13 M NaCl, 2.7 mM KCl, 100 mM Na_2HPO_4, and 1.76 mM KH_2PO_4 (pH 7.4), and immediately disrupted with a French press in buffer A [50 mM Tris-HCl (pH 7.5), 1 mM EDTA, 5 mM $MgCl_2$, and 1 mM glutamine] containing 1.0 mM phenylmethanesulfonyl fluoride. The cell extract was obtained by centrifugation at 27000*g* for 1 h. Streptomycin sulfate was added to a final concentration of 10 mg/mL to precipitate DNA. After centrifugation at 27000*g* for 30 min, the supernatant was applied to a 1.9 cm × 20 cm column of DEAE-Sepharose equilibrated with buffer A. The column was washed with 300 mL of buffer A, followed by 300 mL of buffer A and 0.14 M ammonium sulfate. The enzyme was eluted by a 600 mL linear salt gradient, 0.14 to 0.3 M ammonium sulfate in buffer A. Fractions containing the major protein peak detected by A_{278} were pooled. The enzyme was concentrated to 15−20 mg/mL by centrifugal ultrafiltration using a Centriprep concentrator. Ammonium sulfate was removed by dialysis against 10 mM Tris-HCl (pH 7.5). The total purification was completed in about 36 h, at which time the enzyme was assayed for activity and then stored at −20 °C. The enzyme yield was approximately 200 mg from 2 L of culture. The purity was approximately 95% as judged by SDS−polyacrylamide gel electrophoresis. The initial specific activity of the wild-type enzyme using the glutaminase assay was 60−65 units/mg of protein. The activity decreased by 50% during storage at −20 °C over a period of 1 month, but complete stabilization has recently been obtained by addition of 15% glycerol.[2]

For purification of GAR synthetase, *E. coli* B834 cells containing plasmid were grown in Luria broth containing 50 μg/mL kanamycin for 16−18 h at 37 °C. Cells from 2 L of medium were suspended in 4 mL of buffer B [25 mM $KHPO_4$ (pH 7.5), 5 mM EDTA, 5 mM DTT, and 10% glycerol] per gram of cells and disrupted with a French press. Cell extract was obtained by centrifugation for 30 min at 27000*g*. Protamine sulfate (5 mg per gram of cells) was added to precipitate DNA. After centrifugation at 27000*g* for 30 min, the supernatant was applied to a 1.9 cm × 20 cm DEAE-Sepharose column equilibrated with buffer B. The column was washed with 400 mL of buffer B, and then 400 mL of buffer B and 0.1 M KCl, and eluted with an 800 mL linear gradient of 0.1 to 0.5 M KCl in buffer B. The major enzyme peak, determined by A_{280}, was collected and concentrated to approximately 60 mg/mL by centrifugal ultrafiltration with a Centriprep filter. The protein was stored at −70 °C in buffer B containing 20% glycerol. The enzyme yield was approximately 240 mg from 2 L of culture. The purity was greater than 90% as estimated by SDS−polyacrylamide gel electrophoresis. The specific activity measured in a coupled assay with glutamine PRPP amidotransferase to provide a saturating concentration of PRA was 35 μmol min^{-1} (mg of protein)$^{-1}$.

Enzyme Assays. Three assays were used for glutamine PRPP amidotransferase. The reaction shown by eq 1 was assayed by measurement of the amount of either glutamate or PRA. Reactions for the measurement of glutamate production, termed a glutaminase assay, contained 20 mM glutamine, 2.5 mM PRPP, 5 mM $MgCl_2$, 50 mM Tris-HCl (pH 7.5), and approximately 50 ng of enzyme in a final volume of 100 μL. Incubation was carried out for 6 min at 37 °C. The reaction was stopped by heating in a boiling water bath for 1 min, and the amount of glutamate was determined by the glutamate dehydrogenase method (*8*). The extent of PRA production was determined in a coupled assay with GAR synthetase as described previously (*11*) except the buffer pH was 7.5 instead of 8.0. This reaction is termed Gln-PRA. The synthesis of PRA using NH_3 as the substrate (eq 2) was assayed by essentially the same procedure as Gln-PRA except 150 mM NH_4Cl replaced glutamine and the pH of the buffer was 8.5. For all glutamine PRPP amidotransferase assays, 1 unit of activity is defined as the amount of enzyme needed to produce 1 μmol of product per minute. The specific activity is units per milligram of protein. The protein was determined by A_{278} using a value of 8.12 for a 1% solution (*8*).

GAR synthetase activity was assayed in a coupled reaction with a 50-fold excess of glutamine PRPP amidotransferase

[2] A. K. Bera, unpublished results.

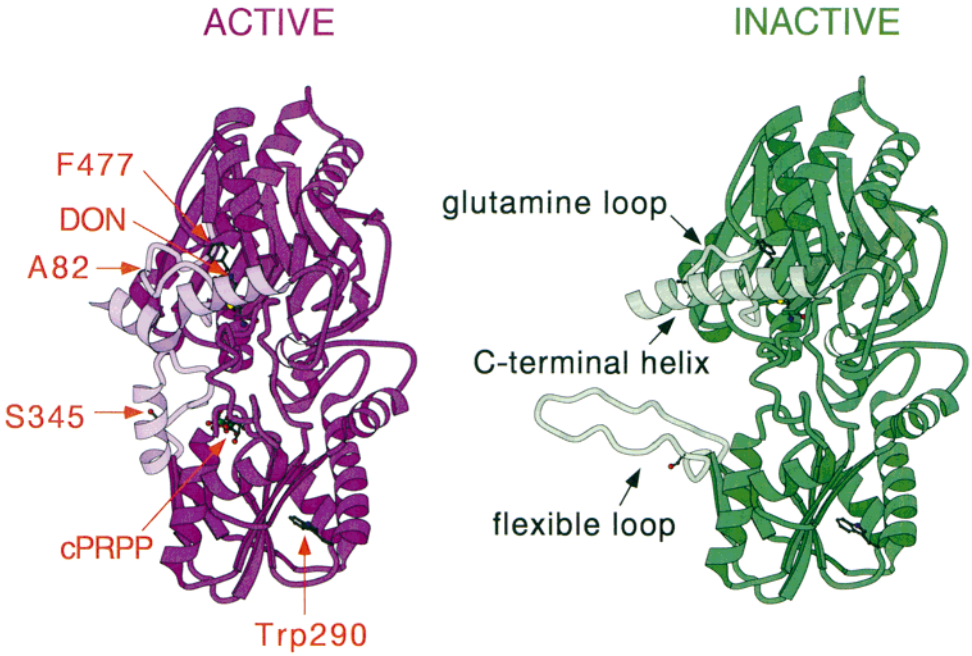

FIGURE 1: Ribbon diagrams of one glutamine PRPP amidotransferase subunit of the enzyme tetramer. (left) Closed, active ternary complex with substrate analogues DON and Mn−cPRPP. The model is available in the Protein Data Bank as file name lecb. (right) Open, inactive conformer without ligands. The model is in the Protein Data Bank as file name lecf. Subunits are drawn in the same orientation with the Ntn glutaminase domain at the top and the PRTase domain at the bottom. Peptides having the largest conformational differences are highlighted and labeled. The position of Trp290 is labeled along with residues in the flexible loop, C-terminal helix, and glutamine loop that were replaced by tryptophan. The figure was modified from that in ref *10*.

to generate PRA substrate. The production of GAR was monitored using [^{14}C]glycine and Dowex 50 chromatography as described by Schendel et al. (*15*). The 40 μL reaction mixture contained 50 mM Tris-HCl (pH 8.0), 1 mg/mL bovine serum albumin, 10 mM MgOAc, 6.25 mM PRPP, 200 mM NH_4Cl, 2 mM [^{14}C]glycine, 2.5 mM ATP, 5 μg of glutamine PRPP amidotransferase, and about 100 ng of GAR synthetase. The incubation was carried out at 37 °C for 4 min.

Steady State Fluorescence. Steady state fluorescence data were obtained using an SLM-8000C spectrofluorimeter at room temperature. A 2.0 mL incubation solution was stirred continuously in a 1.0 cm × 1.0 cm cuvette. The excitation wavelength was set at 300 nm for selective excitation of tryptophan fluorescence. The bandwidths for both excitation and emission monochromators were 4 nm. Spectra were corrected for background and Raman scattering by subtracting buffer spectra containing all ingredients except the enzyme. To monitor fluorescence intensity change with time or for multiple addition of ligands or quencher, the emission wavelength was set to the maximum determined for each specific enzyme, wild type or mutant. A standard incubation mixture contained 10 mM Tris-HCl (pH 7.5), 5 mM $MgCl_2$, and 1 μM enzyme subunit. When they were added, the concentrations of PRPP and glutamine were 1.5 and 20 mM, respectively. To denature the enzyme, it was incubated with 6 M guanidine hydrochloride at 4 °C for 24 h before measurement.

The extent of quenching of tryptophan fluorescence was determined using stock solutions of 5 M acrylamide or 5 M KI containing 0.1 mM sodium dithionite (*16*). The quenching data were plotted according to the Stern−Volmer equation (*17*), $F_o/F = 1 + K_{sv}[Q]$, where F_o and F are the relative fluorescence intensity prior to and after addition of the quenching ligand, respectively, at concentration [Q]. K_{sv} is the Stern−Volmer quenching constant.

To obtain binding constants from ligand titrations, data were fit to the equation $F' = (K_d + F'_{ml}L)/(K_d + L)$ (*18*) using Ultrafit software (Biosoft, Cambridge, U.K.). In this equation, $F' = F/F_o$, where F_o and F are fluorescence intensities in the absence and presence of ligand, respectively; $F'_{ml} = F_{ml}/F_m$, where F_{ml} and F_m are molar fluorescence constants for the enzyme−ligand complex and free enzyme, respectively; L is the ligand concentration; and K_d is the dissociation constant. This equation assumes a single binding site per monomer with no interactions between sites.

Fluorescence Lifetimes. Time-resolved fluorescence measurements were performed in the Purdue University Department of Chemistry laser facility using instrumentation and data collection that have been described previously (*19*). Briefly, excitation was by the pulse method, using a picosecond dye laser pumped by a mode-locked ND:YAG laser (Quantronix 4117E), with dye laser output frequency doubled to provide 295 nm pulses. Emission photons were collected using two emission cutoff filters of >320 and <400 nm. Emission data were collected in duplicate using single-photon counting detected by a Hamamatsu R3809U microchannel plate photomultiplier. Proteins were diluted into 10 mM Tris-HCl buffer (pH 7.5) to a final monomer concentration of 4 μM. Ligands, if present, were at a final concentration of 5 mM $MgCl_2$, 1.5 mM PRPP or 5 mM $MgCl_2$, 1.5 mM PRPP, and 20 mM glutamine. Data were collected at room temperature (approximately 23 °C) and were fit to exponential equations based on a nonlinear least-squares Marquardt algorithm using Ultrafit software. The goodness of fit was determined by reduced χ^2 and weighted residual plot analysis.

Stopped-Flow Fluorescence Kinetics. The pre-steady state kinetics of the ligand binding reactions of glutamine PRPP amidotransferase were examined by measuring changes in the intrinsic tryptophan fluorescence intensity. A Hi-Tech Scientific rapid mixing spectrofluorometer, equipped with a high-intensity xenon arc lamp, was used to follow the reaction. Separate reaction mixing chambers contained enzyme and ligands. The excitation wavelength and the slit width were 295 and 5 mm, respectively. The emitted light was filtered using a cutoff filter (WG 320; 80% transmittance at 320 nm) or passed through a second monochromator set at 350 nm. The reactions were carried out at room temperature (23−25 °C), although for each set of measurements the temperature varied less than 1 °C. The dead time of this instrument is ≤1.5 ms. Typically, 512 time points were collected for varying lengths of time, and usually four or more experiments were averaged. Each averaged data set was then fitted to eqs 4 and 5, shown below, using KinetAsyst2 software from Hi-Tech Limited

$$\Delta F_{obs}(t) = C_1 \exp(-k_{obs}t) + mt + C_0 \quad (4)$$

$$\Delta F_{obs}(t) = C_1 \exp(-k_{obs1}t) + C_2 \exp(-k_{obs2}t) + C_0 \quad (5)$$

where $\Delta F_{obs}(t)$ is the observed fluorescence change (in arbitrary units) at time t, k_{obs1} and k_{obs2} are observed first-order rate constants, C_1 and C_2 are the pre-exponential factors, m is the slope of a zero-order process, and C_0 is the offset for each data set fitting. The regression analysis that was used was based on the Marquardt algorithm procedure.

RESULTS

Construction of Enzymes with Single Tryptophan Residues and Enzymatic Characterization. X-ray structures have defined active and inactive glutamine PRPP amidotransferase states (*6*, *7*). The most dramatic structural change in the transition from the inactive to an active state is an ordering of a PRTase domain flexible loop (residues 326−350) which sequesters the PRPP site from solvent and results in the formation of a 20 Å channel connecting the glutamine and PRPP sites (Figure 1). This structural change is accompanied by a restructuring of the glutamine loop (residues 73−84) and kinking of the adjacent C-terminal α-helix (residues 471−492) (Figure 2) which contribute to activation of the glutamine site for catalysis. To monitor the transitions between inactive and active conformers in solution, we have utilized intrinsic tryptophan fluorescence to report enzyme conformational changes. The strategy was to remove the single tryptophan residue at position 290 in the wild-type enzyme (Figure 1) and to introduce a tryptophan reporter in each of the structural elements involved in the transition from the inactive to the active conformer (Figure 2). It was necessary initially to identify amino acid replacements that were minimally disruptive to enzyme function. Three activities were assayed to characterize the engineered enzymes. The levels of glutamate and PRA production were measured to assay the reaction shown by eq 1. When the amount of glutamate was determined, the assay is referred to as glutaminase (Table 1). With the wild-type enzyme, the hydrolysis of glutamine and the reaction of NH_3 with PRPP are tightly coupled to the synthesis of PRA. The amount of PRA was determined by coupling with an excess of GAR synthetase and measurement of the amount of glycinamide ribonucleotide. This latter assay is termed Gln-PRA in Table 1. The product of the synthesis of PRA using an external source of NH_3 (eq 3) is termed NH_3-PRA in Table 1.

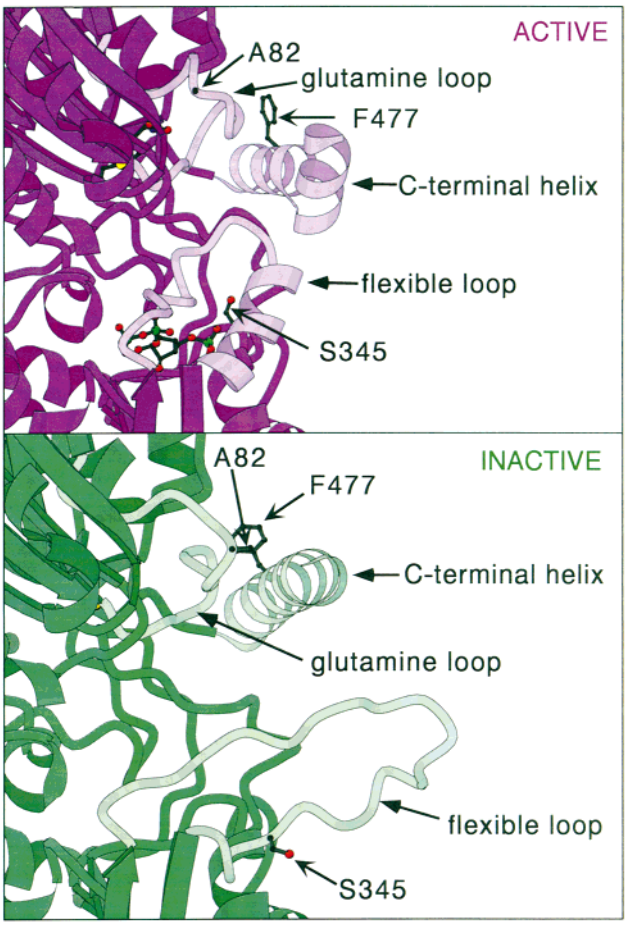

FIGURE 2: Closeup view of peptides involved in the transition between inactive (bottom) and active (top) states. Views are approximately from the backside of Figure 1. The figure was modified from that in ref *10*.

Table 1: Enzyme Activity of Tryptophan Mutants

enzyme[a]	glutaminase (units/mg)	Gln-PRA (units/mg)	NH_3-PRA (units/mg)
Trp290 (wild-type)	63.2 ± 3.1	60.1 ± 4.0	149 ± 3.0
Phe290	66.5 ± 2.2	58.8 ± 4.6	153 ± 7.3
Trp345	41.6 ± 3.5	43.0 ± 3.1	96.4 ± 3.3
Ser1 Trp345	ND[b]	ND	80.1 ± 6.7
Trp477	55.9 ± 5.3	41.7 ± 2.8	140 ± 6.4
Ser1 Trp477	ND	ND	178 ± 5.5
Trp82	13.4 ± 0.03	14.7 ± 0.2	28.7 ± 2.7
Ser1 Trp82	ND	ND	148 ± 7.2

[a] All Trp mutants have phenylalanine at position 290. [b] Not detected.

Data in Table 1 summarize the activities of the enzymes constructed for this study. As a result of a small improvement in enzyme over production and rapid purification, the specific activity of the wild-type enzyme, designated Trp290 in line 1 of Table 1, was more than 2 times higher than that obtained previously (*11*). NH_3-PRA activity was 2−3 times higher than glutaminase or Gln-PRA activities, consistent with earlier work (*8*, *11*). Replacement of Trp290 with Phe (Phe290, Table 1, line 2) had no significant effect on the three glutamine PRPP amidotransferase activities that were measured. Small differences between glutaminase and Gln-

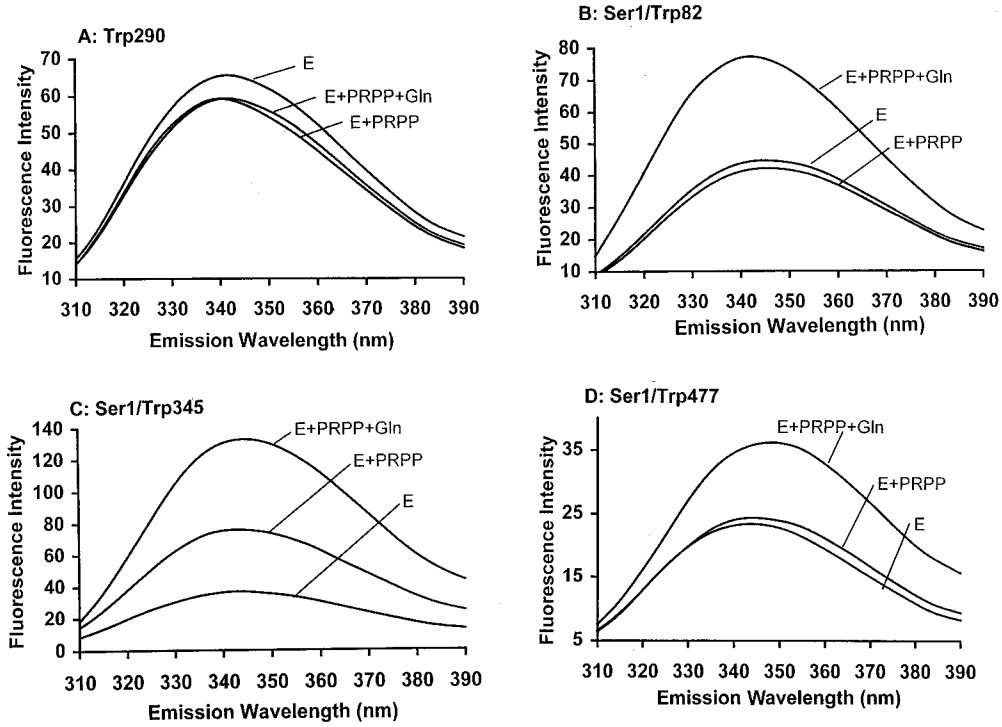

FIGURE 3: Fluorescence emission spectra of enzymes having a single tryptophan reporter. Trp290 represents the wild-type enzyme.

PRA activities are seen in Table 1 for the wild type and some of the mutant enzymes. These departures from 1:1 stoichiometry were not investigated since they have no bearing upon the analyses that were carried out.

A tryptophan residue was inserted by site-directed mutagenesis into the flexible loop, C-terminal helix, and glutamine loop of the tryptophan-free Phe290 enzyme to give Trp345, Trp477, and Trp82 enzymes, respectively. These positions are shown in Figure 2. Since Trp290 was replaced, these three enzymes contain a single tryptophan at the indicated position. The Trp345 and Trp477 enzymes retained more than 60% of the activity seen in the wild-type Trp290 and tryptophan-free Phe290 enzymes (Table 1). The Trp82 glutamine loop mutant enzyme was partially disabled, having only about 20% of the wild-type activity as a result of introducing a bulky side chain into a seven-amino acid stretch of loop structure that contains only alanine, serine, and glycine residues. A number of the Trp insertions that were constructed were not useful. Enzymes with flexible loop reporters F334W and I335W were inactive, and binding of substrates did not perturb fluorescence emission in enzymes with V330W and Q339W reporters. In several enzymes, including those with D471W, Y474W, F475W, and F477W replacements in the C-terminal helix, fluorescence emission was not perturbed by binding of substrates.

To obtain fluorescence measurements of an enzyme−PRPP−glutamine ternary complex without complications of enzyme turnover, a C1S mutation was incorporated into each of the tryptophan mutants. Cys1 is the nucleophile that is required for glutamine hydrolysis. The three Ser1 mutants had no detectable activity with glutamine as a substrate but exhibited between 50 and 120% of the NH_3-PRA activity of the parental Phe290 enzyme (Table 1). A possible reason for the low NH_3-PRA activity in the Trp82 enzyme and the 5-fold increase in this activity when Ser1 was incorporated into the Trp82 enzyme is considered in the Discussion. Overall, the data in Table 1 support the conclusion that functional enzymes were engineered each having a single tryptophan reporter group in one of the three key structural elements involved in the transition between inactive and active states.

Fluorescence Spectra of Wild-Type and Engineered Enzymes. To monitor in solution the changes in conformation that accompany substrate binding seen in the X-ray structures, steady state fluorescence emission spectra were determined for enzymes with single tryptophan residues. Tryptophan fluorescence is sensitive to the polarity of the microenvironment in a protein. As a result, fluorescence changes in proteins containing a single tryptophan reporter group have been used to monitor conformational changes (*20*−*24*). Since Trp290 in the wild-type enzyme is in an α-helix (residues 270−291) that does not undergo a significant structure change in the transition from the inactive to the active state (Figure 1), the Trp290 enzyme served as a fluorescence control. Panel A in Figure 3 shows that conversion from the inactive to the active conformation by addition of substrates had little effect on the fluorescence emission spectrum of the enzyme. Similar results were obtained for the Ser1 Trp290 enzyme (data not shown). Thus, binding of ligands had no significant effect on the Trp reporter fluorescence in the absence of a local conformational change.

In contrast to the effect of ligands on the Trp290 reporter, the fluorescence intensity of the Ser1 Trp345 enzyme increased 2-fold upon addition of PRPP and a further 1.5-fold in the presence of PRPP and glutamine (Figure 3C). Addition of glutamine by itself had no effect on the fluorescence of the enzyme (not shown), consistent with earlier work showing that intermediate reactions of glutamine require binding of PRPP (*8*). These results demonstrate a change in the microenvironment of Trp345 upon binding PRPP, consistent with an ordering of the flexible loop in

which the solvent accessibility to the fluorophore is decreased. This fluorescence change identifies an intermediate conformation for the enzyme·PRPP complex. An X-ray structure has not yet been obtained for this intermediate conformational state. The further increase in fluorescence intensity when glutamine binds to the enzyme·PRPP complex indicates additional repositioning of Trp345. Unlike PRPP, glutamine does not interact directly with the flexible loop, yet the fluorescence enhancement suggests that a change in flexible loop conformation results from glutamine binding. Equilibration of the amidotransferase between the inactive and active states seen in X-ray crystal structures is likely complex, involving multiple intermediate conformations. Nevertheless, it is useful to refer to three functional states each having a specific fluorescence emission spectrum: I, ligand-free, inactive enzyme; II, enzyme·PRPP complex having NH_3-PRA activity; and III, enzyme·PRPP·glutamine ternary complex having Gln-PRA activity.

The tryptophan reporter in the glutamine loop also exhibits fluorescence changes that are indicative of different conformations in the enzyme−substrate ternary complex (Figure 3). Binding of PRPP was not detected by fluorescence emission of the Trp82 glutamine loop reporter as seen in Figure 3B. Even though Trp82 did not report a response of the glutamine loop to PRPP binding, the enzyme·PRPP complex was poised for glutamine binding. This is shown by the nearly 2-fold fluorescence increase in response to binding of glutamine to the enzyme·PRPP complex (Figure 3B).

The C-terminal helix, residues 471−492, contacts the glutamine loop and with a peptide sequence of residues 404−420 helps to close off the glutamine site in the inactive conformation (*6*). In the active conformation, an interaction of the flexible loop with the glutamine loop results in bending of the C-terminal helix (Figure 2). A F477W replacement inserted a tryptophan into the C-terminal helix to monitor conformational changes between the inactive and active states. The fluorescence spectra of the Trp477 enzyme with or without PRPP were very similar (Figure 3D), suggesting that the C-terminal helix was not in its final state III active conformation after PRPP binding. Addition of glutamine to the enzyme·PRPP complex resulted in a 1.5-fold increase in fluorescence intensity and a 5 nm red shift, reflecting a movement of the C-terminal helix.

Time-Resolved Fluorescence. The fluorescence lifetime was determined for the Trp290 wild-type protein and each of the mutant enzymes, and data are summarized in Table 2. Representative fluorescence decay data are shown in Figure 4 for the Ser1 Trp477 enzyme. Two decay times were required to obtain the best fit, determined with reduced χ^2 values and visual examination of the weighted residuals, for all enzyme−ligand combinations except for the Ser1 Trp345 enzyme ternary complex (data not shown). Data for the Ser1 Trp345 ternary complex were fit best to a single-exponential decay. Interpretation of multiple lifetimes is complex, and individual lifetimes cannot be ascribed to specific conformers. However, intensity-weighted average lifetimes (τ_{av}) were calculated (Table 2) and were used to determine bimolecular quenching constants (k_q) from steady state quenching data (K_{sv}) as given in Table 2 and described in the next section.

Fluorescence Quenching. The environment of a specific tryptophan residue can also be evaluated by its accessibility

Table 2: Average Fluorescence Lifetimes and Quenching Constants for Single Tryptophan Enzyme−Ligand Combinations[a]

enzyme	τ_{av}[b] (ns)	χ^2[c]	K_{sv} (M^{-1})	k_q ($\times 10^9$ M^{-1} s^{-1})
Ser1 Trp345	3.21	1.06	10.1	3.15
Ser1 Trp345 and PRPP	4.87	1.09	8.33	1.71
Ser1 Trp345, PRPP, and Gln	7.59	1.03	5.55	0.73
Ser1 Trp345 and 6 M Gdn-HCl			10.9	
Ser1 Trp82	2.56	1.10	9.23	3.61
Ser1 Trp82 and PRPP	2.89	1.10	8.22	2.84
Ser1 Trp82, PRPP, and Gln	2.44	1.10	3.18	1.30
Ser1 Trp82 and 6 M Gdn-HCl			10.1	
Ser1 Trp477	1.77	1.10	4.32	2.44
Ser1 Trp477 and PRPP	2.34	1.09	4.40	1.88
Ser1 Trp477, PRPP, and Gln	4.29	1.02	5.90	1.38
Ser1 Trp477 and 6 M Gdn-HCl			10.7	
Trp290	1.96	1.08	5.68	2.90
Trp290 and PRPP	1.83	1.06	6.48	3.54
Trp290, DON, and PRPP[d]	2.23	1.04	6.39	2.87
Trp290 and 6 M Gdn-HCl			10.4	

[a] K_{sv} was determined from linear Stern−Volmer plots. The linear correlation coefficient for all plots was >0.99. The quenching rate (k_q) was calculated from the relationship $k_q = K_{sv}/\tau_{av}$. [b] Average tryptophan lifetime was calculated from the equation $\tau_{av} = \Sigma\alpha_i\tau_i 2/\Sigma\alpha_i\tau_i$, where τ and α are the lifetime (nanoseconds) and associated fractional contribution to the total emission intensity, respectively. [c] χ^2 is the goodness of fit parameter. [d] The DON glutamine analogue permits formation of a stable ternary complex. With the wild-type enzyme, glutamine and PRPP would react to form products.

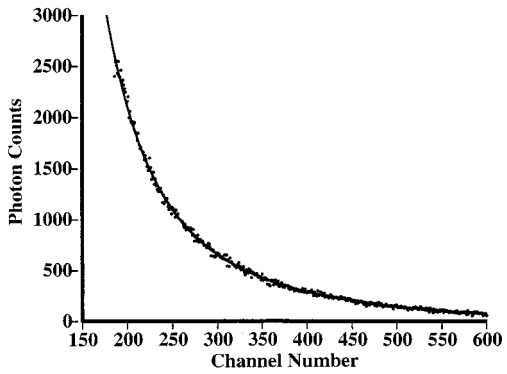

FIGURE 4: Fluorescence decay of the Ser1 Trp477 enzyme. The channel width was 31 ns^{-1}. Data were fit to eq 5 having two exponential terms. The enzyme concentration was 4 μM monomer in 10 mM Tris-HCl (pH 7.5).

to small molecule fluorescence quenchers. Stern−Volmer constants (K_{sv}) for quenching of Trp290, Trp82, and Trp345 enzymes by acrylamide and the Trp477 enzyme by iodide were determined from linear plots with correlation coefficients of >0.99 and are given in Table 2. Iodide was used for quenching of the Trp477 enzyme because of anomolous results with acrylamide that were independent of ligand binding (data not shown). To provide a reference for the relative accessibility to quencher, K_{sv} values were also determined for enzymes denatured by guanidine hydrochloride. K_{sv} values for fully exposed tryptophan residues were between 10.1 and 10.9 in the denatured enzymes. Decreased Stern−Volmer constants in the native enzymes are consistent with reduced accessibility of tryptophan to the quencher. To evaluate more critically the accessibility of the tryptophan reporters, bimolecular quenching constants (k_q) were calculated from values of K_{sv} and average fluorescence lifetime data and are given in Table 2. The bimolecular quenching constants are intermediate between the values reported (*25*)

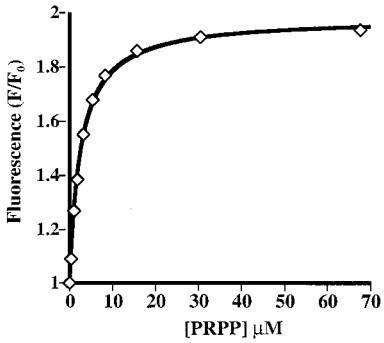

FIGURE 5: Determination of the binding constant for PRPP by fluorescence titration. The Ser1 Trp345 enzyme (2.0 μM subunits) was titrated with PRPP at room temperature. Data were corrected for dilution and free ligand concentration when the concentrations of total ligand and enzyme were similar. Data were fit to the equation given in Experimental Procedures. F is the observed fluorescence intensity after addition of ligand and F_0 the initial fluorescence in the absence of ligand.

for a deeply buried residue ($<0.05 \times 10^9$ M^{-1} s^{-1} in azurin) to near maximal exposure in a randomly coiled peptide (adrenocorticotropin, 4.2×10^9 M^{-1} s^{-1}). As seen in Table 2, substrate ligands have little or no effect on the rate of reaction of quencher with Trp290. However, PRPP and PRPP with glutamine significantly decreased k_q in enzymes with a tryptophan reporter in the flexible loop (Trp345), the glutamine loop (Trp82), and the C-terminal helix (Trp477). These data thus support the sequential repositioning by PRPP and glutamine of Trp345 in the flexible loop, Trp82 in the glutamine loop, and Trp477 in the C-terminal helix.

Substrate Binding Constants. The Trp345 fluorescence signal was used to determine binding constants for substrates. Figure 5 shows the results of a fluorescence titration of the Ser1 Trp345 enzyme with PRPP at room temperature. A similar titration with glutamine was carried out in the presence of saturating PRPP (data not shown). The estimated K_d values for PRPP and glutamine are 2 and 195 μM, respectively. These K_d values are much smaller than K_m values of 50−70 μM for PRPP and 1.5−2.0 mM for glutamine, suggesting that two or more steps are involved in substrate binding.

Rapid Kinetics of PRPP·Enzyme Binary Complex Formation. While equilibrium binding experiments are useful for assessing the number and type of enzyme−substrate-bound states, they do not directly address the sequence and kinetics of steps leading to the formation of enzyme−substrate complexes. This information was sought using stopped-flow fluorescence to follow the formation of enzyme−substrate binary and ternary complexes.

Pre-steady state kinetics for the formation of the binary E·PRPP complex were studied by measuring the intrinsic tryptophan fluorescence changes of the flexible loop reporter in the Ser1 Trp345 enzyme. Figure 6A shows the fluorescence time course of a rapid mixing experiment, where the PRPP concentration was substantially greater than the enzyme concentration. A double-exponential equation (eq 5) gave the best fit to the data depicted in Figure 6A. Both k_{obs1} and k_{obs2} varied independently over a 40-fold range in enzyme concentrations (not shown), which is expected for a reaction first-order in enzyme. k_{obs1} and k_{obs2} were dependent upon the PRPP concentration. The value of k_{obs1} increased linearly with PRPP concentration with no sign of saturation

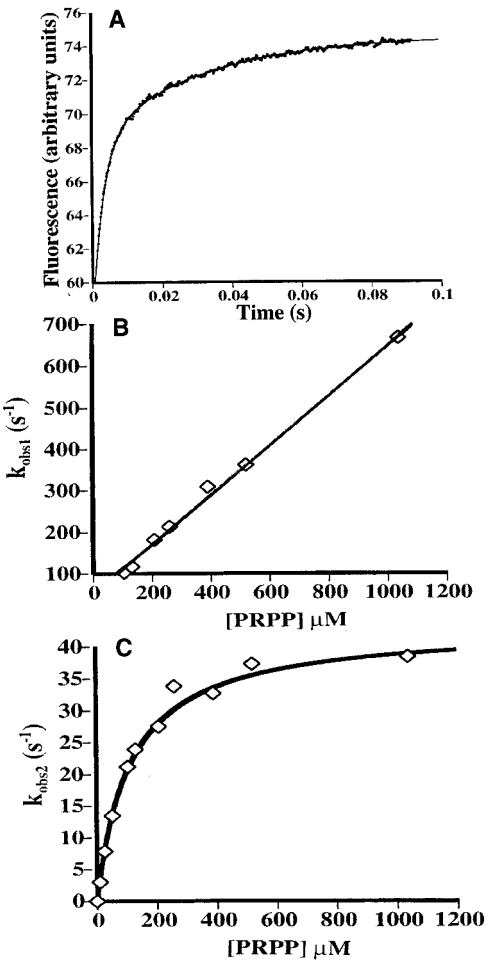

FIGURE 6: Pre-steady state kinetics for binding of PRPP to the Ser 1 Trp345 enzyme. (A) Fluorescence time course for binding of PRPP. The fluorescence enhancement was measured after rapid mixing of 4 μM Ser1 Trp345 enzyme in subunits in 50 mM Tris-HCl (pH 7.5) with 1.5 mM PRPP, 10 mM $MgCl_2$, and 50 mM Tris-HCl (pH 7.5) at room temperature. The curve, fit to eq 5, is superimposed on the data points. (B) Dependence of the pseudo-first-order rate constant, k_{obs1}, obtained from eq 5 on PRPP concentration. Data were fit to eq 6. (C) The observed rate constant, k_{obs2}, obtained from eq 5 was plotted against the PRPP concentration. The line was fit to the data points using eq 7 by nonlinear least-squares regression.

(Figure 6B), while that for k_{obs2} increased hyperbolically with PRPP concentration (Figure 6C). These results are consistent with, at least, a two-step reaction, as shown in Scheme 1, where the complex E·PRPP further isomerizes to form E*·PRPP.

Scheme 1

$$E + PRPP \underset{k_{-1}}{\overset{k_1}{\rightleftharpoons}} E\cdot PRPP \underset{k_{-i}}{\overset{k_i}{\rightleftharpoons}} E^*\cdot PRPP$$

The linear relationship between k_{obs1} and PRPP concentration is consistent with a bimolecular reaction shown by the first step in Scheme 1, where k_{obs1} should vary according to eq 6 where k_1 and k_{-1} are the forward and reverse rate constants, respectively.

$$k_{obs1} = k_1[PRPP] + k_{-1} \quad (6)$$

The results of fitting values for k_{obs1} at different PRPP concentrations to eq 6 are shown in Figure 6B, and the values

Table 3: Equilibrium and Kinetic Rate Constants Obtained from PRPP Binding Studies

pH	k_1[a] ($\times 10^5$ M^{-1} s^{-1})	k_{-1}[a] (s^{-1})	K_1[b] (μM)	k_i[a] (s^{-1})	k_{-i}[a] (s^{-1})	K_i[b]	K_1K_i (μM)	K_d[c] (μM)	k_{cat}[d] (s^{-1})
7.5	6.0	53	88	43	1.5	0.034	2.8	1.9	ND[e]
8.5	4.3	38	88	49	3.0	0.061	5.3	2.6	44

[a] Rate constants derived from pre-stead -state kinetics according to the model shown in Scheme 1. [b] Equilibrium constants calculated from pre-steady state kinetics rate constants; $K_1 = k_{-1}/k_1$, and $K_i = k_{-i}/k_i$. [c] Dissociation constant measured from equilibrium fluorescence titration experiments. [d] NH_3-PRA reaction determined at room temperature. [e] Not determined at pH 7.5. The pH optimum for the NH_3-PRA reaction is ~8.5.

of k_1 and k_{-1} are given in Table 3 (entries for pH 7.5). The association rate constant (k_1) is about 2 orders of magnitude slower than expected. This discrepancy is considered in the Discussion. The value of the calculated dissociation constant, 88 μM for PRPP binding ($K_1 = k_{-1}/k_1$), is about 40-fold larger than the K_d of 1.9 μM estimated from fluorescence titration with PRPP. These data are consistent with Scheme 1 where the isomerization step will pull the equilibrium reaction to the right. The hyperbolic behavior of k_{obs2} with PRPP concentration shown in Figure 6C is also consistent with the two-step mechanism in Scheme 1. The first step, association of E and PRPP, is essentially at equilibrium and is followed by a slow isomerization that gives rise to an additional fluorescence change. Under these conditions, k_{obs2} should vary with PRPP concentration as shown by eq 7, where k_i is the rate constant for isomerization and K is the equilibrium dissociation constant for the first step in Scheme 1.

$$k_{obs2} = k_i[\text{PRPP}]/([\text{PRPP}] + K) \quad (7)$$

Data depicted in Figure 6C were fit to eq 7 by nonlinear regression analysis. The estimates for k_i and K (eq 7) are 43 $\pm$ 1.6 s^{-1} and 110 $\pm$ 12.6 μM, respectively. The value of K is satisfactorily close to the ratio of k_{-1}/k_1 (88 μM), as it should be.

Rapid Kinetics of E·PRPP Decomposition*. The formation of the PRPP·enzyme complex requires Mg^{2+} (*7*, *8*); thus, the dissociation of PRPP from enzyme could be determined by mixing the binary complex with EDTA. This reaction was zero-order in EDTA and first-order in E*·PRPP (data not shown). The time course of fluorescence decay after rapid mixing of EDTA with the PRPP·enzyme complex was fit to eq 4 which involves both a zero-order and a first-order phase (data not shown). The first-order decay rate constant was 1.5 s^{-1} (Table 3). The slow zero-order process seems to involve photo-oxidation of Trp345 as indicated by the slow fluorescence decay of enzyme alone (data not shown). Since the PRPP off-rate was considerably slower than k_{-1} for E·PRPP dissociation (Table 3), the off-rate determined here likely describes k_{-i}, the step from E*·PRPP to E·PRPP. The fact that the value of $(k_{-1}k_{-i})/(k_1k_i)$ or K_1K_i in Table 3 is similar to the K_d determined from the equilibrium PRPP titration (Figure 5) provides independent support for the model in Scheme 1.

Comparison of the Pre-Steady State Rate Constant for Isomerization of E·PRPP with the k_{cat} for NH_3-PRA Formation. A k_{cat} of 43 s^{-1} was determined for the NH_3-PRA reaction at pH 8.5 (which is close to the pH optimum). The rapid kinetics experiments were repeated at pH 8.5, and the rate constants deduced from these experiments are given in Table 3. The values of rate constants do not vary appreciably between pH 7.5 and 8.5. The value of k_i for the isomerization step, 49 s^{-1} at pH 8.5, is not significantly different from that of k_{cat} for the NH_3-PRA reaction. Thus, isomerization of E·PRPP is likely rate-determining for aminolysis of PRPP by NH_3. However, the rates k_1[PRPP] and k_i for the formation of E*·PRPP are larger than the k_{cat} for the Gln-PRA reaction (15.7 s^{-1}, data not shown) at the optimal pH of 7.5, indicating that the rate-limiting step for the Gln-PRA reaction occurs after E*·PRPP formation.

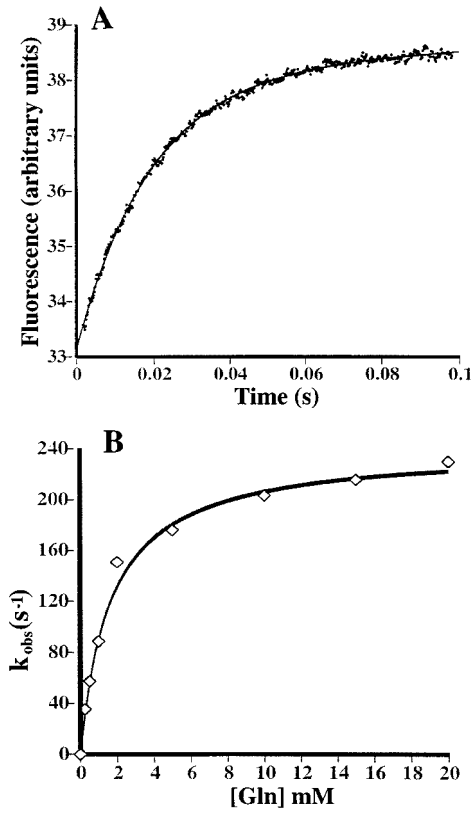

FIGURE 7: Pre-steady state kinetics for binding of glutamine to the Ser1 Trp477 emzyme−PRPP complex. (A) Time course of the fluorescence change. The fluorescence change was initiated by rapid mixing of 1 mM glutamine with 4 μM Ser1 Trp477 enzyme (subunits), 3 mM PRPP, 10 mM $MgCl_2$, and 50 mM Tris-HCl (pH 7.5). Data were fit to eq 4. (B) Effect of glutamine concentration on k_{obs}. The observed rate constants obtained from eq 4 were plotted against the glutamine concentration. The curve was fit to eq 8 by nonlinear least-squares regression.

Rapid Kinetics of Glutamine Binding to E·PRPP*. The kinetics for E·PRPP·Gln ternary complex formation were investigated using both the C-terminal α-helix Trp477 reporter in the glutamine domain (Figure 1) and the PRTase flexible loop Trp345 reporter in the PRPP domain. The Ser1 Trp477 enzyme saturated with PRPP was mixed with excess glutamine relative to enzyme, and a rapid increase in enzyme fluorescence was observed (Figure 7A). In the absence of PRPP, no change in fluorescence was observed (data not shown). These data were best fit to eq 4, which includes both zero- and first-order processes. The slope of the zero-order reaction did not change as a function of glutamine concentration, and this zero-order reaction was therefore not studied further. To investigate the effect of glutamine concentration on k_{obs} for the first-order process, the extent

of binding was determined over the range where the glutamine concentration should saturate the enzyme, 0.25−20 mM. Values of k_{obs} varied hyperbolically as a function of glutamine concentration (Figure 7B). The hyperbolic relationship between k_{obs} and glutamine concentration is consistent with a two-step mechanism shown in Scheme 2 where the first step, formation of

Scheme 2

$$E^{*}\cdot PRPP + Gln \overset{K_{Gln}}{\rightleftharpoons} Gln\cdot E^{*}\cdot PRPP \overset{k_i}{\rightleftharpoons} Gln\cdot E^{\Delta}{}^{*}\cdot PRPP$$

Gln·E*·PRPP is essentially at equilibrium and is followed by a slow isomerization that gives rise to a fluorescence change. Under these conditions, k_{obs} should vary as shown by eq 8 where K_{Gln} is the equilibrium dissociation constant of the first step and k_i is the rate of enzyme isomerization in the second step shown in Scheme 2.

$$k_{obs} = k_i[Gln]/([Gln] + K_{Gln}) \quad (8)$$

Data depicted in Figure 7B were fit to eq 8 by nonlinear regression analysis. The estimated values of K_{Gln} and k_i were 1.7 mM and 220 s^{-1}, respectively. Thus, the kinetic mechanism includes an isomerization step for the glutamine domain upon binding of glutamine, like the isomerization of the PRTase domain upon binding of PRPP. We presume this isomerization of the glutamine domain corresponds to the closing of the glutamine site, to give the conformer seen in the X-ray structure of the ternary complex (Figure 1).

The PRTase flexible loop is also involved in glutamine binding since the fluorescence of the Ser1 Trp345 enzyme·PRPP binary complex also increases when glutamine binds. Thus, the kinetics for ternary complex formation were also determined using the Trp345 flexible loop reporter. These experiments were performed in the same manner as those for glutamine binding to the Ser1 Trp477 enzyme. However, the data in this case were best fit to eq 5, which contains two first-order exponential terms. The values of k_{obs2} for the slow process increased hyperbolically with glutamine concentration and were fit to eq 8. The calculated values for K_{Gln} and k_i were 6.4 mM and 219 s^{-1}, respectively. The values for the isomerization step are identical for the flexible loop and C-terminal helix reporters. It thus appears that both the PRTase flexible loop and the C-terminal α-helix of the glutamine binding domain move synchronously to form the ternary complex. The different K_{Gln} values for Ser1 Trp477 and Ser1 Trp345 enzymes correlate with glutamine K_m values for these enzymes (data not shown). For the fast step, the observed first-order rate constant k_{obs1} also varied as a function of the glutamine concentration, but the rate was too fast to measure with our instrumentation.

DISCUSSION

By incorporating a tryptophan fluorescence probe into each of three positions within the protein that undergo significant structural rearrangements, we established a system for monitoring in solution the glutamine PRPP amidotransferase conformational changes that are needed to coordinate catalysis at the two physically separated active sites. In the ligand-free state I conformer, the C-terminal helix (residues 471−492) of the glutamine domain contacts the glutamine loop (residues 73−84), and together with peptide residues 404−420 contributes to closure of the glutamine site. In this closed structure, Arg73 would not interact with the α-carboxyl group of glutamine, a contact that is essential for high-affinity binding (*11*). In state I, k_{cat}/K_m for a basal PRPP-independent glutaminase activity is less than 0.2% of that for the state III enzyme (Figure 8). In the ligand-free enzyme, the PRTase flexible loop is open and is poorly ordered (*9*, *10*). In this open state, the fluorescence intensity of Trp345 was relatively low (Figure 3C) and the Stern−Volmer constant for quenching of Trp345 by acrylamide was similar to that for the denatured enzyme, indicating maximal accessibility. These fluorescence properties are all consistent with a relatively solvent-exposed environment for the Trp345 flexible loop reporter that is consistent with the X-ray structure model.

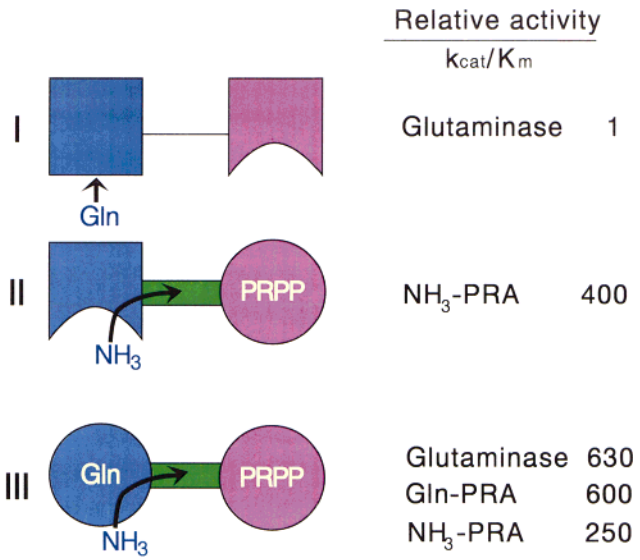

FIGURE 8: Model for three enzyme states. In state I, the glutamine site is closed, the PRPP site is open, and the two sites are separated by a solvent accessible space. This ligand-free conformer has a low basal glutaminase activity (*11*). The value of k_{cat}/K_m is set to 1.0. Binding of PRPP leads to state II in which the PRPP site is closed, the glutamine site is open, and an NH_3 channel connects the two sites. It is proposed that NH_3 enters the channel from the open glutamine site. In the state III ternary complex, the enzyme is poised for glutamine hydrolysis and coupled synthesis of PRA. External NH_3 can enter the channel from the closed glutamine site. Relative enzyme activities were calculated from Table 1.

Binding of PRPP to the enzyme resulted in an increased fluorescence signal of the Trp345 reporter and a reduced rate for fluorescence quenching by acrylamide, changes that suggest a reorganization of the flexible loop. The kinetics for this process were consistent with a mechanism of at least two steps in which rapid equilibrium binding of PRPP is followed by a slow isomerization of the enzyme·PRPP complex. The value of the rate constant, k_1, that was determined for the first step of the binding process shown in Scheme 1 was 6×10^5 M^{-1} s^{-1} at pH 7.5 (Table 3). This rate is clearly slower than that expected for a diffusion-controlled step such as binding of PRPP to an accessible site in the ligand-free enzyme. The slower-than-expected rate constant may be due to a two-step process that appears as a single step, as has been observed for the binding of GlcNac-β(1−4)-GlcNac to lysozyme (*26*, *27*). If the apparent initial PRPP association step shown in Scheme 1 were a two-step

process, the slope of the plot in Figure 6B would not give k_1 (eq 6) according to Scheme 1 but would represent a more complex term (*26*). As a result, the apparent association constant k_1 obtained from Figure 6B would be slower than the true association rate constant. Thus, the overall two-step binding process shown by Scheme 1 may require a third step as shown in Scheme 3. In this scheme, the rate of the first step is diffusion-controlled and steps 2 and 3 are rapid and slow isomerizations, respectively.

Scheme 3

$$E + PRPP \rightleftharpoons E{\cdot}PRPP \rightleftharpoons E^1{\cdot}PRPP \underset{k_{-i}}{\overset{k_i}{\rightleftharpoons}} E^*{\cdot}PRPP$$

The rate constant k_i for the final enzyme isomerization of 49 s^{-1} at pH 8.5 is likely to be rate-limiting for the NH_3-PRA reaction. This isomerization should correspond to the ordering of the flexible loop that must precede the reaction of NH_3 with PRPP. Rate-limiting conformational changes have been observed previously for several enzymes, including triosephosphate isomerase (*28*) and dihydrofolate reductase (*29*).

Although the fluorescence emission of the Trp477 and Trp82 reporters was not perturbed by binding of PRPP to the enzyme, decreased rates for fluorescence quenching by small molecules are consistent with a structural change in the glutamine domain. This change in accessibility to quencher may report the opening of the glutamine site and the repositioning of Arg73, steps that are required for binding of glutamine to the enzyme·PRPP complex. Overall, the measurements of steady state fluorescence of the three Trp reporters define a state II conformer which is an intermediate in the transition between the two structurally defined end point conformers. Crystals of the state II wild-type enzyme, trapped with cPRPP, are isomorphous with state III crystals (cPRPP and DON) but diffract very poorly (*9*). Thus, in overall structure, state II is more similar to state III than to state I.

Binding of glutamine to the state II enzyme·PRPP complex completes the conformational transition and leads to state III. Tryptophan reporter groups in the PRTase flexible loop, glutamine loop, and C-terminal helix all exhibit increases in fluorescence and significant decreases in their quench constants for state III compared to state II, consistent with conformational changes. The kinetics of glutamine binding, investigated with Trp345 and Trp477 reporters, are complex. The Trp477 C-terminal α-helix reporter detected zero-order and first-order processes in glutamine binding. The role of the zero-order process in the conformational transition is not understood. The Trp345 flexible loop reporter monitored two first-order steps. The initial first-order process was too fast to study, and it was not defined. However, the concentration dependence of the first-order rate constant for glutamine binding to the Trp477 enzyme and the slower of the two rate constants for glutamine binding to the Trp345 enzyme are consistent with a minimum two-step binding mechanism shown by Scheme 2, in which fast equilibrium binding of glutamine is followed by a slow isomerization step. Since the rates for isomerization were the same whether monitored by the PRTase flexible loop reporter or the C-terminal α-helix glutaminase domain reporter, the conformational changes in these structural elements are likely to occur in concert to yield the ternary complex. The rates of the two steps leading to the ternary complex are faster than the k_{cat} for the Gln-PRA reaction. Thus, some step in the reaction mechanism other than these conformational changes is rate-limiting for glutamine hydrolysis.

Two lines of evidence indicate that binding of PRPP to the enzyme initiates a key signaling step that coordinates catalysis at the glutamine and PRPP sites. First, no glutamine binding was detected in the absence of PRPP, indicating that closing and reorganization of the PRTase flexible loop are required for glutamine binding. Second, fluorescence changes in the Trp345 reporter, reflecting changes in the flexible loop conformation, were monitored when glutamine was bound to the state II enzyme·PRPP conformer. Thus, the PRTase flexible loop has a role in glutamine binding in the absence of a direct interaction with glutamine. It is therefore apparent that the conformational changes resulting from PRPP binding to the PRTase active site enable glutamine to bind and undergo hydrolysis. In both state I and state III, the glutamine loop and C-terminal helix act as a gate and latch to keep the glutamine site closed (*9*). According to the current model, movement of the flexible loop in response to PRPP binding initiates a series of changes beginning with contact of Ile335 in the flexible loop and Tyr74 in the glutamine loop. A steric clash of these invariant side chains is the only incompatibility between the closed state III flexible loop and the state I glutamine loop. The resulting restructuring of the glutamine loop is propagated to the C-terminal helix, a change that could open the gate to permit access of glutamine to the site. The conformational change in the glutamine loop as a result of PRPP binding, mediated by the Ile335−Tyr74 interaction, also has another important consequence. The position of Arg73 is determined by the glutamine loop conformation. An important salt bridge between Arg73 and the α-carboxylate of glutamine is missing in state I (*11*) and is present in state III (*7*). The importance of the Ile335−Tyr74 interaction for glutamine binding has been established by mutational studies to be reported elsewhere.[3]

The low NH_3-PRA activity of the Trp82 enzyme (Table 1) has important implications. We propose that insertion of Trp82 into the glutamine loop obstructs entry of NH_3 into the NH_3 channel. In the Ser1 Trp82 enzyme, the glutamine loop has more freedom to move because of the loss of a Tyr74 NH−Cys1 Sγ hydrogen bond. This hydrogen bond cannot form with Ser1 Oγ. Thus, Trp82 could be less effective in hindering NH_3 entry, and NH_3-PRA activity was restored in the Ser1 Trp82 enzyme (Table 1). This interpretation leads to the important conclusion that external as well as internal NH_3 used for the NH_3-PRA reaction in state II enters the NH_3 channel via the glutamine site, as depicted schematically in Figure 8. It also leads to the prediction that the NH_3-PRA reaction might be partially impaired in the state III enzyme, where the glutamine site is known to be closed and occupied. In accord with this prediction, the rate of the NH_3-PRA reaction is modestly higher in state II, having a presumably open glutamine site, than in state III. It was found that glutamine inhibited by 2-fold the NH_3-PRA activity of the Ser1 Trp345 enzyme (data not given).

We have not considered in this work the structural transitions that are required for release of products. It is

[3] A. K. Bera, S. Chen, J. L. Smith, and H. Zalkin, unpublished data.

anticipated that a return of the PRTase flexible loop to a less ordered state is required to open the PRTase site for release of PRA and PP_i and the glutamine site for release of glutamate.

E. coli carbamoyl phosphate synthetase also contains physically separated active sites for glutamine hydrolysis and carbamate synthesis that are connected by an NH_3 channel (*30)*. A 3 order of magnitude increase in the rate of glutamine hydrolysis upon addition of ATP and bicarbonate is indicative of the allosteric communication between the sites (*31*). Structural changes required for the intersubunit signaling have yet to be reported.

ACKNOWLEDGMENT

This work would not have been possible without the instrumentation that was made available by colleagues at Purdue University. Richard Dilley and V. Jo Davison provided access to spectrofluorimeters for steady state and rapid mixing experiments. Stanislov D. Zakharov provided instruction on the use of the SLM-8000C spectrofluorimeter. Special gratitude is expressed to Kenneth Haber, Department of Chemistry, for assembly and operation of the complex instrumentation for measuring tryptophan fluorescence lifetimes and for his dedicated efforts in optimizing operating conditions. We thank Fred E. Lytle for critical analyses of fluorescence lifetime data, Tanya E. S. Dahms for important discussions of the fluorescence data, and Aloke Kumar Bera for numerous enthusiastic discussions during the course of the research.

REFERENCES

1. Zalkin, H., and Smith, J. L. (1998) *Adv. Enzymol. Relat. Areas Mol. Biol. 72*, 87−144.
2. Brannigan, J. A., Dodson, G., Duggleby, H. J., Moody, P. C. E., Smith, J. L., Tomchick, D. R., and Murzin, A. G. (1995) *Nature 378*, 416−419.
3. Eads, J. C., Ozturk, D., Wexler, T. B., Grubmeyer, C., and Sacchettini, J. C. (1997) *Structure 5*, 47−58.
4. Zalkin, H. (1993) *Adv. Enzymol. Relat. Areas Mol. Biol. 66*, 203−309.
5. Smith, J. L., Zaluzec, E. J., Wery, J.-P., Niu, L., Switzer, R. L., Zalkin, H., and Satow, Y. (1994) *Science 264*, 1427−1433.
6. Muchmore, C. R. A., Krahn, J. M., Kim, J. H., Zalkin, H., and Smith, J. L. (1998) *Protein Sci. 7*, 39−51.
7. Krahn, J. M., Kim, J. H., Burns, M. R., Parry, R. J., Zalkin, H., and Smith, J. L. (1997) *Biochemistry 36*, 11061−11068.
8. Messenger, L. J., and Zalkin, H. (1979) *J. Biol. Chem. 254*, 3382−3392.
9. Krahn, J. M. (1998) Ph.D. Dissertation, Purdue University, West Lafayette, IN.
10. Smith, J. L. (1998) *Curr. Opin. Struct. Biol. 8*, 686−694.
11. Kim, J. H., Krahn, J. M., Tomchick, D. R., Smith, J. L., and Zalkin, H. (1996) *J. Biol. Chem. 271*, 15549−15557.
12. Kunkel, T. A., Roberts, J. D., and Koukour, R. A. (1987) *Methods Enzymol. 154*, 367−382.
13. Shen, Y., Rudolph, J., Stern, M., Stubbe, S., Flannigan, K. A., and Smith, J. M. (1990) *Biochemistry 29*, 218−227.
14. Doherty, A. J., Ashford, S. R., Brannigan, J. A., and Wigley, D. B. (1995) *Nucleic Acids Res. 23*, 2074−2075.
15. Schendel, F. J., Cheng, Y. S., Otvos, J. D., Wehrli, S., and Stubbe, J. (1988) *Biochemistry 27*, 2614−2623.
16. Lehrer, S. S. (1971) *Biochemistry 10*, 3254−3263.
17. Lakowicz, J. R. (1983) in *Principles of Fluorescence Spectroscopy*, pp 257−301, Plenum Press, New York.
18. Eftink, M. R. (1997) *Methods Enzymol. 278*, 221−257.
19. Pokalsky, C., Wick, P., Harms, E., Lytle, F. E., and Van Etten, R. L. (1995) *J. Biol. Chem. 270*, 3809−3815.
20. Stole, E., and Bryant, F. R. (1994) *J. Biol. Chem. 269*, 7919−7925.
21. Watanabe, F., Jameson, D. M., and Uyeda, K. (1996) *Protein Sci. 5*, 904−913.
22. Barry, J. K., and Matthews, K. S. (1997) *Biochemistry 36*, 15632−15642.
23. Zhou, T., and Rosen, B. P. (1997) *J. Biol. Chem. 272*, 19731−19737.
24. Hildebrand, E. L., and Grossman, L. (1998) *J. Biol. Chem. 273*, 7818−7827.
25. Eftink, M. R., and Ghiron, C. A. (1976) *Biochemistry 15*, 672−680.
26. Fersht, A. R. (1985) *Enzyme Structure and Mechanism*, pp 121−153, W. H. Freeman, San Francisco.
27. Boldo, J. H., Halford, S. E., Patt, S. L., and Sykes, B. D. (1975) *Biochemistry 14*, 1893−1899.
28. Rose, I. A., and Iyengar, R. (1982) *Biochemistry 21*, 1591−1597.
29. Falzone, C. J., Wright, P. E., and Benkovic, S. J. (1994) *Biochemistry 33*, 439−442.
30. Thoden, J. B., Holden, H. M., Wesenberg, G., Raushel, F. M., and Rayment, I. (1997) *Biochemistry 36*, 6305−6316.
31. Miles, B. W., Banzon, J. A., and Raushel, F. M. (1998) *Biochemistry 37*, 16773−16779.

BI991060O